NANO LETTERS

Letter

pubs.acs.org/NanoLett

Yield and Shape Selection of Graphene Nanoislands Grown on Ni(111)

M. Olle,*[,†] G. Ceballos,*[,†] D. Serrate,[‡,§] and P. Gambardella[†,∥]

[†]Catalan Institute of Nanotechnology (ICN) and Universitat Autònoma de Barcelona, UAB Campus, E-08193 Bellaterra (Barcelona), Spain

[‡]INA-LMA, University of Zaragoza, 50018 Zaragoza, Spain

[§]Dpto. de Física de la Materia Condensada, University of Zaragoza, 50009 Zaragoza, Spain

[∥]Institució Catalana de Recerca i Estudis Avançats (ICREA), E-08010 Barcelona, Spain

ABSTRACT: The catalytic decomposition of hydrocarbons on transition-metal surfaces has attracted increasing interest as a method to prepare high quality graphene layers. Here, we study the optimal reaction path for the preparation of graphene nanoislands of selected shape using controlled decomposition of propene on Ni(111). Scanning tunneling microscopy performed at different stages of the reaction provides insight into the temperature and dose-dependent growth of graphene islands, which precedes the formation of monolayer graphene. The effect of postreaction annealing on the morphology of the islands is studied. By adjusting the initial propene dose, reaction temperature, and postannealing procedure, islands with a triangular or hexagonal shape can be selectively obtained.

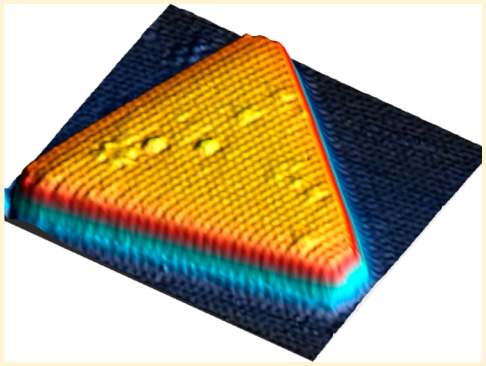

KEYWORDS: *Graphene, Ni(111), self-assembly, scanning tunneling microscopy*

The epitaxial growth of graphene on transition-metal substrates represents one of the most promising routes for the production of large-area graphene sheets,[1−6] offering significant advantages over the micromechanical cleavage of highly oriented pyrolitic graphite.[7] Different factors such as the type of substrate, carbon precursor, temperature, and pressure have been shown to affect the growth mechanism.[8−10] However, although graphene epitaxy on metals has been studied for a long time,[8,11] knowledge about the nucleation and growth kinetics, which ultimately determine its quality and structure, is still limited.[12] Progress in this field is hindered by the presence of several rate-limiting processes that compete with each other toward the growth of graphene, such as desorption of the carbon precursor, the formation of carbide phases, and C dissolution into the bulk.[6,13−16] It is therefore an open question whether graphene epitaxy can reach the level of insight and sophistication typical of metal[17] and semiconductor[18] growth.

A related issue concerns the possibility of fine-tuning the epitaxial process to induce the self-assembly of graphene nanostructures of well-defined shape and dimensions. Owing to confinement and edge effects, graphene quantum dots have attracted considerable interest for applications in nanoelectronics[19,20] as well as for fundamental reasons.[21−23] Moreover, theoretical investigations predict the appearance of intriguing magnetic properties on the edges of graphene islands,[24−26] where zigzag edges may possess finite magnetic moments that add up in triangular islands but compensate exactly in hexagonal ones.[24]

Most efforts to produce graphene nanostructures with controlled shape rely on top-down techniques such as electron beam lithography,[27] nanoimprint,[28] and scanning probe lithography,[29,30] for which the edge quality is not always satisfactory. On metals, graphene nanoislands have been obtained by surface segregation of bulk C,[1] direct evaporation of C, and thermal dissociation of hydrocarbons on Ir(111),[31] Ru(0001),[32] Co(0001),[22] and Cu(001).[33] In most of such cases, the islands grow with irregular shapes and present a broad size distribution. Attempts to steer the growth process toward shape and size selection have so far been successful only for nanoribbons[34] and very small graphene-like clusters with dimensions in the range of 1 to 25 nm^2.[35−37]

In this paper, we develop a method to grow graphene nanoislands on a Ni(111) surface with selected shape, dimensions up to 300 nm^2, and optimal edge quality. Using scanning tunneling microscopy, we present a systematic investigation of the growth parameters that affect the yield, structure, size, and shape of submonolayer C islands on Ni(111) following the deposition of propene (C_3H_6) at room temperature. We show that sequential control of the catalytic decomposition of a fixed dose of propene, reaction temper-

Received: March 6, 2012
Revised: August 6, 2012
Published: August 17, 2012

ature, and postannealing procedure leads to the formation of graphene islands with either triangular or hexagonal shape, zigzag edges, and partial size selection.

All the experiments were performed on a Ni(111) single-crystal surface kept in a ultrahigh vacuum (UHV) chamber with a base pressure of 3×10^{-10} mbar. The crystal surface was cleaned by repeated cycles of Ar+ sputtering followed by annealing at 800 °C for 1 min. The surface temperature was measured throughout the experiment using a pyrometer (IMPAC IGA 140) with ±25 °C accuracy at 450 °C and ±2 at 500 °C. Topographic images of the surface were obtained using a variable-temperature scanning tunneling microscope (STM) and processed using the WSxM software.[38] After the cleaning procedure, the Ni crystal presented less than 0.01 monolayers (ML) of carbon contamination in the form of nickel carbide. Such a minor contamination did not affect the growth process in a measurable way, as verified by the absence of graphene nucleation upon annealing to 500 °C. The procedure used to prepare the graphene nanoislands is divided in three steps: (1) dosing of propene on Ni(111) at room temperature (RT); (2) decomposition of propene and formation of ordered C phases at the reaction temperature $350 \leq T_R \leq 600$ °C; (3) postannealing of graphene nanoislands at temperature $450 \leq T_A \leq 650$ °C. During the first two steps propene decomposes and forms graphene; during the third step, surface and bulk C diffusion compete, determining the yield as well as the average size and shape of graphene nanoislands. The initial dose of propene (D) is expressed in Langmuirs, calculated by time-integration of the partial pressure of propene. Once D has reached its programmed value and the chamber has recovered its base pressure, the sample is heated up to T_R using a constant heating rate of 12 °C/s. After reaching T_R, the sample temperature is kept stable within ±5 °C for a time $t = t_R$, after which heating is stopped and the sample allowed to cool at a rate of 1.7 °C/s until RT, before transfer into the STM. This sequence is repeated on a clean surface for every value of T_R investigated in this work. During the postannealing process the graphene nanoislands are heated from RT to T_A for a time t_A, after which the sample is cooled and observed by STM.

In order to describe the critical steps of graphene growth, we have systematically varied the values of the reaction parameters T_R, D, and t_R. We start by describing the effect of T_R, which turns out to be the most important reaction parameter, at constant dose (D = 1 L) and reaction time (t_R = 1 min). Figure 1 shows representative STM images of the submonolayer growth process obtained after step 2. As observed in Figure 1a, relatively large round islands form already at T_R = 350 °C. These islands are 2.5 Å high and present a characteristic stripe pattern on their upper surface. The same pattern can be observed on the terraces, covering the entire crystal surface and forming a multidomain striped phase. High-resolution STM images of this pattern on flat terraces (Figure 1e, left) reveal the atomic structure of nickel carbide, as previously observed by Klink et al.[15] and confirmed by low energy electron diffraction. Similar results are obtained for reactions up to T_R = 400 °C.

At T_R = 450 °C (Figure 1b) the nickel carbide islands are still present, but the surface is only partially covered by the nickel carbide phase, which is now single-domain and concentrated on the upper part of the surface steps (light blue area on the right-hand side of Figure 2b). Atomic resolution images (Figure 1e) taken on an area equivalent to the dark blue region of Figure 1b reveal an hexagonal lattice with interatomic distance identical to

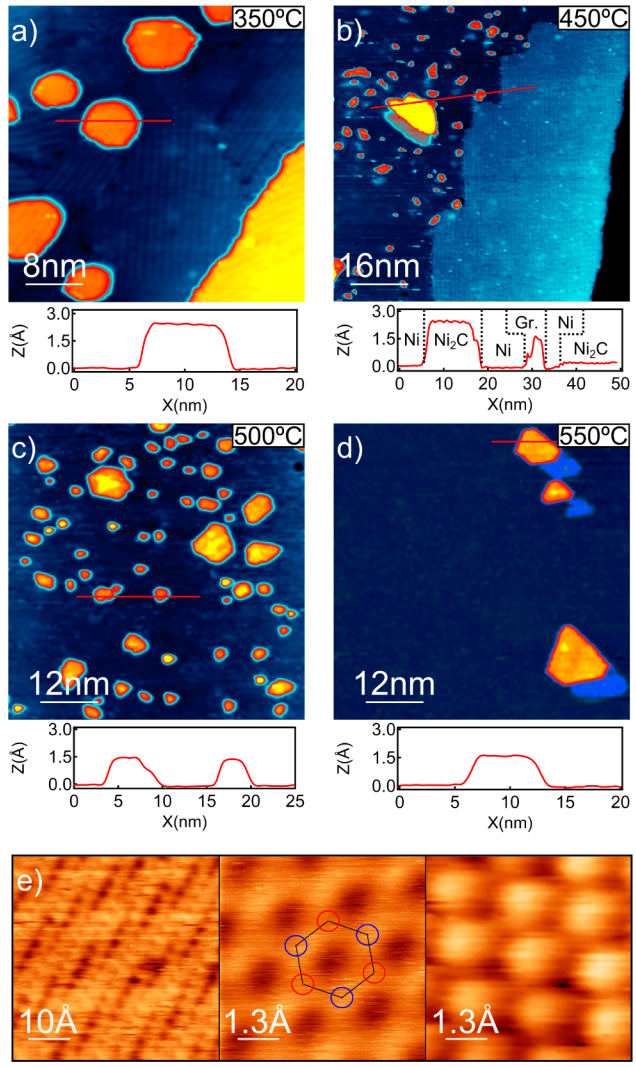

Figure 1. STM images of the surface topography following preparations with D = 1 L, t_R = 1 min and (a) T_R = 350 °C, (b) T_R = 450 °C, (c) T_R = 500 °C, and (d) T_R = 550 °C. Images b and d are affected by a double tip effect. (e) Atomic resolution images of nickel carbide (left), graphene (center), and Ni(111) (right).

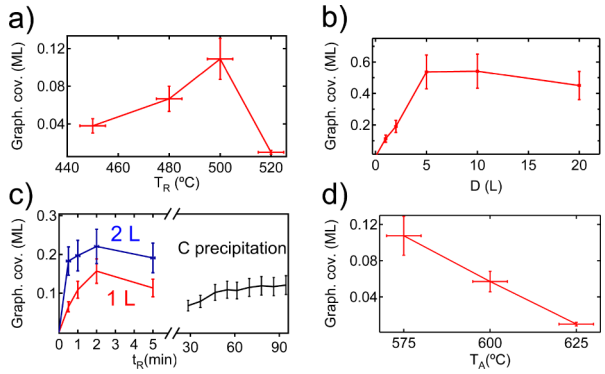

Figure 2. Graphene coverage as a function of (a) T_R at constant D = 1 L and t_R = 1 min, (b) D at constant T_R = 500 °C and t_R = 5 min, (c) t_R at D = 1 (red), 2 (blue) L, and T_R = 500 °C, (d) T_A at constant D = 2 L, t_R = 1 min, T_R = 500 °C, and t_A = 10 min. The black curve in (c) shows the slow increase of the graphene coverage of a sample maintained at 500 °C for up to 90 min due to carbon precipitation.

dx.doi.org/10.1021/nl300897m | Nano Lett. 2012, 12, 4431−4436

that of pristine Ni(111). In these regions of carbide free Ni, we observe small islands of irregular shape with a height of 1.5 Å, which represent the first stage of graphene formation on this surface.

Figure 1c shows the preparation at T_R = 500 °C. The Ni carbide phase has entirely dissolved. On the other hand, we observe a broad distribution of islands with compact but rather irregular shape, which have the same height (1.5 Å) as the small islands observed in Figure 1b. High-resolution images of these islands (Figure 1e, center) show the 3-fold symmetry typical of the monolayer graphene structure on Ni(111).[15] The images also show the presence of a second phase enclosed in some of the graphene islands, which we attribute to Ni atoms from its apparent height (2.1 Å). As T_R increases up to 550 °C, we observe that the density of graphene islands has reduced drastically (Figure 1d) and that the islands present a more regular shape compared to Figure 1b,c. Above 600 °C, we observe no graphene formation and the Ni surface appears clean and homogeneous.

Clearly, there are large differences in graphene yield depending on T_R. Figure 2a shows the graphene coverage estimated from the STM images at different temperatures. In such analysis, we did not consider the contribution of islands smaller than 1 nm^2 and of the Ni atoms enclosed in graphene, which amount to about 0.02 of a clean Ni monolayer. We observe that the graphene yield peaks at T_R = 500 °C and decreases steeply already at 520 °C. Graphene formation starts at around 450 °C as the Ni carbide phase recedes. Our results show that annealing a sample covered with Ni carbide for 1 min at 500 °C yields a clean Ni(111) surface with no traces of either graphene or carbide. Thus, the carbide phase does not transform directly into graphene. This is in agreement with the results of Lahiri et al.,[6] which showed that C atoms first dissolve into the bulk at 480 °C, whereas nucleation of graphene from reverse C diffusion to the surface occurs on a time scale of hours.

The growth process as a function of T_R is summarized below. At temperatures below 400 °C, propene reacts with Ni surface atoms to form nickel carbide, which is in agreement with previous observations.[13] The Ni carbide phase observed at T_R = 450 °C is most probably formed during the heating ramp, as the carbide starts to decompose around 400 °C[39] and our data indicate that the atomic mobility is high enough to restructure the carbide domains above this temperature. As mentioned above, the carbide phase does not contribute to the formation of graphene but rather diffuses into the bulk upon increasing T_R to 500 °C. Graphene formation therefore occurs above 400 °C in the presence of C atoms directly dissociating from propene. This explains why monolayer graphene is usually grown by dosing hydrocarbons directly at high temperature. Above this point, the reaction rate decreases abruptly, which can be explained by the onset of propene desorption from the surface before the reaction can take place. We thus find that the optimal reaction temperature to grow graphene on Ni(111) is 500 °C, whereas dosing at RT allows for reproducible submonolayer control of the graphene coverage.

The relationship between the dose and final graphene coverage has been studied at T_R = 500 °C and t_R =5 min to ensure that a maximal amount of graphene is formed and that all the propene molecules have reacted with the surface. Figure 2b shows that the coverage of graphene increases linearly with the propene dose up to about 0.5 ML between 1 and 5 L. The saturation value depends on the competition between propene dissociation and desorption, which prevents the formation of a full graphene ML at constant dose. The increase in coverage is also accompanied by a change in morphology of the graphene. Below 0.1 ML, we observe isolate nanoislands of different sizes, whereas at larger coverage the islands start to coalesce, becoming large and irregular. Samples with D < 0.5 L, are not included in Figure 2b due to the low reproducibility of the graphene yield: most of preparations with D = 0.5 L present no graphene islands, whereas for some of them the graphene coverage is lower than expected, around 0.01 ML. This behavior can be understood if we assume that the critical island size to catalyze the growth of graphene on metals is a C_5 cluster, as proposed by Zangwill and Vvedensky,[12] implying that fluctuations of the density of C atoms around a minimum threshold value are critical to stabilize the growth of graphene.

Our study shows that the reaction time has also significant effects on the final amount of graphene, as expected for a kinetically controlled process. Figure 2c shows that the graphene coverage increases with t_R. For $t_R \leq 1$ min, the coverage increase rapidly with an average growth rate of 8×10^{-2} ML/min and reaches saturation after 2 min at constant dose (D = 1 L) and temperature (T_R = 500 °C). To study the effect of temperature at long time scales, a sample with a low initial coverage of graphene (0.06 ML) was kept at 500 °C for up to 90 min and observed by STM at the same temperature. We found that the graphene coverage increases slowly with time with a growth rate of about 8×10^{-4} ML/min (Figure 2c). Since propene has entirely desorbed at this temperature, such a small growth rate is attributed to carbon diffusion from the bulk. We thus conclude that graphene growth occurs in two different regimes. The first one ($t_R \leq 5$ min) is characterized by a high growth rate and attributed to carbon obtained directly from the propene reaction, whereas the second regime is characterized by a very low growth rate and is attributed to carbon precipitation from the bulk.

A common feature of the graphene islands prepared according to the method described above is the irregularity of sizes and shapes, which seems to be inherent to the graphene growth process. STM images obtained for long reactions (t_R > 5 min), further show that the island density, morphology, and size change with time. This motivated us to investigate systematically to what extent the average size and shape of the islands can be controlled through postannealing, once the graphene reaction is complete. We thus fixed T_R = 500 °C to ensure graphene formation and avoid nickel carbide contamination and t_R = 5 min for complete graphene formation. In order to obtain isolated islands, we used a dose of 1 L to prepare samples with T_A < 600, and D = 2 L for samples prepared with T_A = 600 and 625 °C to compensate for the loss of graphene due to diffusion into the bulk occurring above 575 °C (see Figure 2d). Figure 3a−d shows the influence of postannealing at T_A = 450−650 °C for a time t_A = 10−20 min (3rd step). Figure 3e,g reports the statistical analysis of the island size distribution derived from STM images acquired before (blue sticks) and after postannealing (red sticks). In both cases, we find that the island size (S) follows a gamma distribution function $P(S) = [\alpha^M/\Gamma(M)]e^{-\alpha S}\, S^{M-1}$, where Γ is the gamma function, α is a scale parameter, M is the shape parameter governing disorder, and the average island size is given by $\langle S \rangle = M/\alpha$.[40,41] The limit M = 1 represents the exponential distribution expected for random events. Prior to postannealing, we obtain M = 1.2, indicating that the simple decomposition of propene does not lead to the self-assembly of

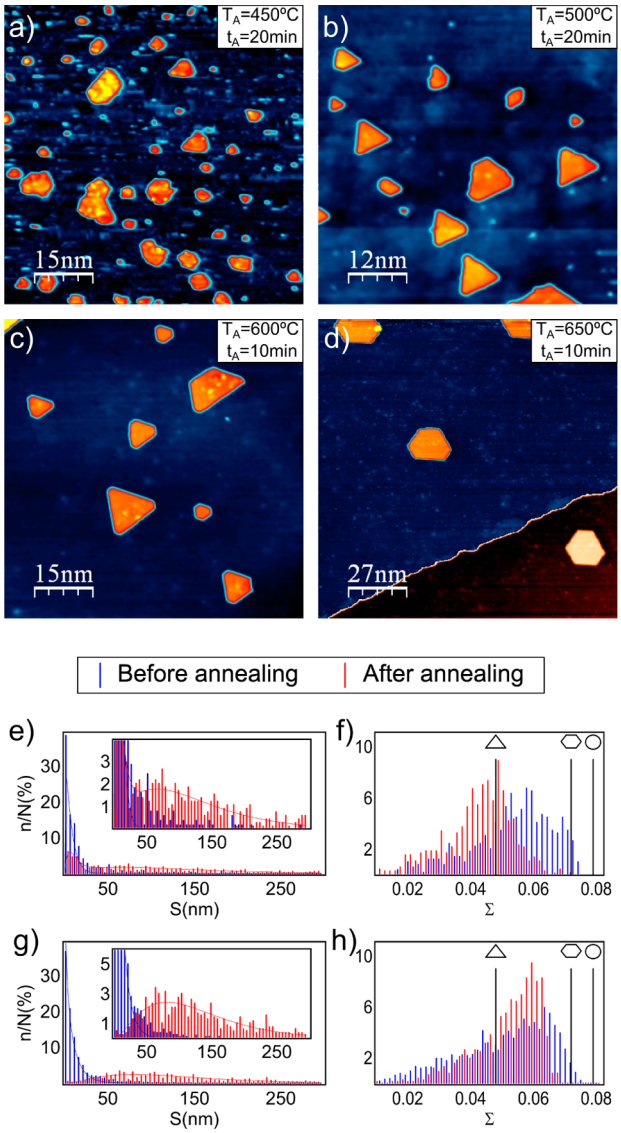

Figure 3. Size and shape distribution of graphene nanoislands as a function of postannealing. All samples are prepared with T_R = 500 °C and t_R = 5 min. Representative STM images are shown for (a) D = 1 L, T_A = 450 °C, and t_A = 20 min. (b) D = 1 L, T_A = 500 °C, and t_A = 20 min. (c) D = 2 L, T_A = 600 °C, and t_A = 10 min. (d) D = 2 L, T_A = 650 °C, and t_A = 10 min. (e–h) Size and shape histograms of islands obtained before (blue sticks) and after (red sticks) postannealing at T_A = 500 °C (e,f) and T_A = 650 °C (g,h).

graphene islands with a preferred size. Following postannealing, we find that the distribution changes from exponential to a peaked function with increasing T_A, leading to $M = 2.8 \pm 0.3$ at T_A = 650 °C and a 10-fold increase of the average island size from about 10 to 120 nm^2.

STM images also show that, besides affecting the island size distribution, postannealing induces significant changes of the island shape. Figure 3a shows the results of the annealing at T_A = 450 °C and t_A = 20 min. The edge of the islands remains irregular and no appreciable edge reorganization is observed. At this temperature the island structure is stable since no change in the island morphology is observed as a function of t_A. A major change of the average island morphology is observed for $T_A \geq$ 500 °C. Figure 3b shows that the larger islands assume a triangular shape after prolonged annealing at 500 °C. At the same time, the size distribution peaks at S = 100 nm^2 while the number of smaller islands decreases significantly (Figure 3e). Statistical analysis of the shape parameter (Σ), defined as the area of each island divided by its perimeter squared reveals that most islands evolve from a round irregular shape ($0.048 < \Sigma \leq 1/4\pi$) toward a triangular shape (Σ = 0.048) (Figure 3f). Atomic resolution STM images (Figure 4a) further show that the triangle edges are now smooth zigzag edges oriented parallel to the $[1\bar{1}0]$, $[\bar{1}01]$ and $[01\bar{1}]$ directions of the Ni(111) surface. As can be observed in the scheme reported in Figure 4b, the edge type is determined by the 1 × 1 stacking of graphene on Ni(111): zigzag edges follow the $[1\bar{1}0]$, $[\bar{1}01]$ and $[01\bar{1}]$ directions whereas armchair edges follow the $[2\bar{1}\bar{1}]$, $[\bar{1}2\bar{1}]$ and $[\bar{1}\,\bar{1}\,2]$ directions. In Figure 4b, we assume a top-fcc stacking for illustrative purposes, although the conclusions obtained for the edge configuration are valid for any 1 × 1 stacking configurations. Upon increasing T_A to 600 °C, we observe that most of the islands present truncated corners. The transition from equilateral to truncated triangles is associated to the different growth rates of the islands along the $[11\bar{2}]$ and $[\bar{1}\bar{1}2]$ high-symmetry directions of Ni, in analogy with epitaxial metal systems.[42,43] For a given stacking, along these high-symmetry directions the island edges atoms assume either a top or hollow configuration with respect to the substrate atoms and consequently different kinetic barriers to annex new C atoms. A change in the temperature will directly affect these barriers and therefore the growth rate. This process culminates in the formation of hexagonal islands as T_A reaches 650 °C, as shown in Figure 3d, as the growth rate equilibrates in both directions. We note that at this temperature the island density is very low owing to graphene lost to C migration into bulk Ni. Although the number of islands is not enough to collect a statistic

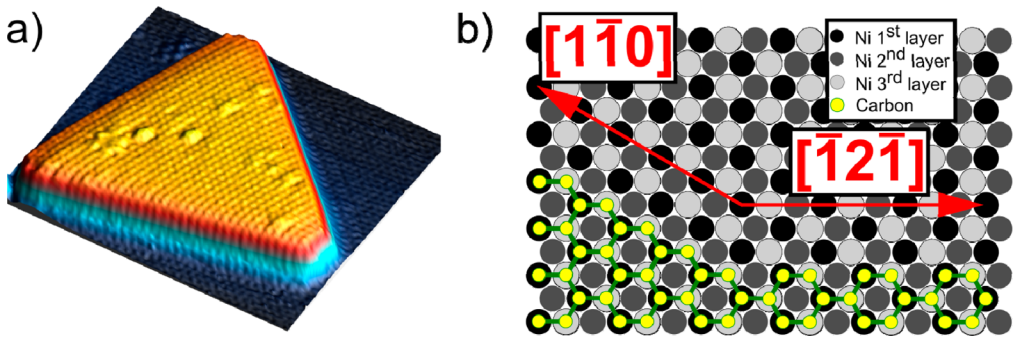

Figure 4. (a) Three-dimensional rendering of an atomic resolution STM image of a triangular island of graphene on Ni(111). (b) Model of the atomic structure of graphene edges on the Ni(111) surface with 1 × 1 stacking.

dx.doi.org/10.1021/nl300897m | Nano Lett. 2012, 12, 4431–4436

comparable to Figure 3e, we observe that all the small islands have completely disappeared at this temperature and that the average size of the hexagons is about 130 nm^2. Figure 3h shows that after postannealing the Σ distribution narrows around an intermediate value between triangles (Σ = 0.048) and hexagons (Σ = 0.072), representing hexagonal islands with unequal edge length.

Epitaxial graphene islands grown on close-packed metal surfaces by decomposition of hydrocarbons usually present broad shape and size distributions.[1,9,31,32] Inducing the self-assembly of graphene nanoislands appears to be particularly difficult due to the need of optimizing several contrasting processes, such as hydrocarbon pyrolysis against desorption, graphene against carbide formation, and edge and surface diffusion of C atoms against bulk diffusion. To summarize our systematic investigation of the growth parameters governing the formation of graphene on Ni(111), we found that the reaction temperature, dose, and postnucleation annealing of the substrate must be sequentially optimized in order to minimize the width of the size and shape distribution of nanosized graphene islands. We developed a method to grow relatively large graphene nanoislands of selected shape on Ni(111). This method is based on the preadsorption of a fixed dose of propene on Ni at RT, followed by heating up to 500 °C, which yields the maximum amount of graphene per dose unit but irregular islands. Lower reaction temperatures favor the formation of nickel carbide, whereas larger temperatures favor fast propene desorption. Annealing time and dose determine the amount of graphene formed. The graphene coverage increases proportionally to the dose up to D = 5 L, after which it saturates to about 0.5 ML. In the final postannealing step, irregular graphene islands undergo a thermal shape selection process, while the smallest islands vanish due to ripening and C migration into the bulk. We showed that by varying the annealing temperature between 500 and 650 °C we can induce the formation of islands larger than 100 nm^2 with either triangular or hexagonal shape. These islands present good structural quality and straight zigzag edges.

■ AUTHOR INFORMATION

Corresponding Author

*E-mail: (M.O.) marc.olle@icn.cat; (G.C.) gustavo.ceballos@icn.cat.

Notes

The authors declare no competing financial interest.

■ ACKNOWLEDGMENTS

This work was partially supported by the Ministerio de Ciencia y Innovación (MAT2010-15659), the Agència de Gestió d'Ajuts Universitaris i de Recerca (2009 SGR 695) and TRAIN2 (SOE2/P1/E280) cofinanced by the Programa Operativo de Cooperación Territorial SUDOE 2007-2013.

■ REFERENCES

(1) Sutter, P. W.; Flege, J.-I.; Sutter, E. A. Epitaxial graphene on ruthenium. *Nat. Mater.* **2008**, *7* (5), 406−411.
(2) Grüneis, A.; Vyalikh, D. V. Tunable hybridization between electronic states of graphene and a metal surface. *Phys. Rev. B* **2008**, *77* (19), 193401.
(3) Pan, Y.; et al. Highly Ordered, Millimeter-Scale, Continuous, Single-Crystalline Graphene Monolayer Formed on Ru (0001). *Adv. Mater.* **2009**, *21* (27), 2777−2780.
(4) Gao, L.; Guest, J. R.; Guisinger, N. P. Epitaxial Graphene on Cu(111). *Nano Lett.* **2010**, *10* (9), 3512−3516.
(5) Günther, S.; et al. Single Terrace Growth of Graphene on a Metal Surface. *Nano Lett.* **2011**, *11* (5), 1895−1900.
(6) Lahiri, J.; et al. Graphene Growth on Ni(111) by Transformation of a Surface Carbide. *Nano Lett.* **2011**, *11* (2), 518−522.
(7) Geim, A. K. Graphene: Status and Prospects. *Science* **2009**, *324* (5934), 1530−1534.
(8) Wintterlin, J.; Bocquet, M. L. Graphene on metal surfaces. *Surf. Sci.* **2009**, *603* (10−12), 1841−1852.
(9) Loginova, E.; et al. Factors influencing graphene growth on metal surfaces. *New J. Phys.* **2009**, *11* (6), 063046.
(10) Sun, Z.; et al. Growth of graphene from solid carbon sources. *Nature* **2010**, *468* (7323), 549−552.
(11) Gall, N. R.; Rut'kov, E. V.; Tontegode, A. Y. Two-Dimensional Graphite Films on Metals and Their Intercalation. *Int. J. Mod. Phys. B* **1997**, *11* (16), 1865.
(12) Zangwill, A.; Vvedensky, D. D. Novel Growth Mechanism of Epitaxial Graphene on Metals. *Nano Lett.* **2011**, *11* (5), 2092−2095.
(13) Grüneis, A.; Kummer, K.; Vyalikh, D. V. Dynamics of graphene growth on a metal surface: a time-dependent photoemission study. *New J. Phys.* **2009**, *11* (7), 073050.
(14) Jacobson, P.; et al. Nickel Carbide as a Source of Grain Rotation in Epitaxial Graphene. *ACS Nano* **2012**, *6* (4), 3564−3572.
(15) Klink, C.; et al. An STM study of carbon-induced structures on Ni(111): evidence for a carbidic-phase clock reconstruction. *Surf. Sci.* **1995**, *342* (1−3), 250−260.
(16) Eizenberg, M.; Blakely, J. M. Carbon monolayer phase condensation on Ni(111). *Surf. Sci.* **1979**, *82* (1), 228−236.
(17) Brune, H. Microscopic view of epitaxial metal growth: nucleation and aggregation. *Surf. Sci. Rep.* **1998**, *31* (4−6), 125−229.
(18) Shiraki, Y.; Sakai, A. Fabrication technology of SiGe heterostructures and their properties. *Surf. Sci. Rep.* **2005**, *59* (7−8), 153−207.
(19) Ponomarenko, L. A.; et al. Chaotic Dirac Billiard in Graphene Quantum Dots. *Science* **2008**, *320* (5874), 356−358.
(20) Ritter, K. A.; Lyding, J. W. The influence of edge structure on the electronic properties of graphene quantum dots and nanoribbons. *Nat. Mater.* **2009**, *8* (3), 235−242.
(21) Hämäläinen, S. K.; et al. Quantum-Confined Electronic States in Atomically Well-Defined Graphene Nanostructures. *Phys. Rev. Lett.* **2011**, *107* (23), 236803.
(22) Eom, D.; et al. Structure and Electronic Properties of Graphene Nanoislands on Co(0001). *Nano Lett.* **2009**, *9* (8), 2844−2848.
(23) Phark, S.-h.; et al. Direct Observation of Electron Confinement in Epitaxial Graphene Nanoislands. *ACS Nano* **2011**, *5* (10), 8162−8166.
(24) Fernández-Rossier, J.; Palacios, J. Magnetism in Graphene Nanoislands. *Phys. Rev. Lett.* **2007**, *99*, 177204.
(25) Yazyev, O. V.; Katsnelson, M. I. Magnetic Correlations at Graphene Edges: Basis for Novel Spintronics Devices. *Phys. Rev. Lett.* **2008**, *100* (4), 047209.
(26) Yang, H.-X.; et al. Inducing and optimizing magnetism in graphene nanomeshes. *Phys. Rev. B* **2011**, *84* (21), 214404.
(27) Duan, H.; et al. Preparing patterned carbonaceous nanostructures directly by overexposure of PMMA using electron-beam lithography. *Nanotechnology* **2009**, *20* (13), 135306.
(28) Liang, X.; et al. Formation of Bandgap and Subbands in Graphene Nanomeshes with Sub-10 nm Ribbon Width Fabricated via Nanoimprint Lithography. *Nano Lett.* **2010**, *10* (7), 2454−2460.
(29) Puddy, R. K.; et al. Atomic force microscope nanolithography of graphene: Cuts, pseudocuts, and tip current measurements. *Appl. Phys. Lett.* **2011**, *98* (13), 133120.
(30) Masubuchi, S.; et al. Fabrication of graphene nanoribbon by local anodic oxidation lithography using atomic force microscope. *Appl. Phys. Lett.* **2009**, *94* (8), 082107.
(31) N'Diaye, A. T.; et al. Structure of epitaxial graphene on Ir(111). *New J. Phys.* **2008**, *10* (4), 043033.

(32) Donner, K.; Jakob, P. Structural properties and site specific interactions of Pt with the graphene/Ru(0001) moiré overlayer. *J. Chem. Phys.* **2009**, *131*, 164701.
(33) Wofford, J. M.; et al. Graphene Islands on Cu Foils: The Interplay between Shape, Orientation, and Defects. *Nano Lett.* **2010**, *10* (12), 4890−4896.
(34) Cai, J.; et al. Atomically precise bottom-up fabrication of graphene nanoribbons. *Nature* **2010**, *466* (7305), 470−473.
(35) Wang, B.; et al. Size-Selective Carbon Nanoclusters as Precursors to the Growth of Epitaxial Graphene. *Nano Lett.* **2011**, *11* (2), 424−430.
(36) Lu, J.; et al. Transforming C60 molecules into graphene quantum dots. *Nat. Nantechnol.* **2011**, *6* (4), 247−252.
(37) Cui, Y.; et al. Formation of identical-size graphene nanoclusters on Ru(0001). *Chem. Commun.* **2011**, *47* (5), 1470−1472.
(38) Horcas, I.; et al. WSXM: A software for scanning probe microscopy and a tool for nanotechnology. *Rev. Sci. Instrum.* **2007**, *78*, 1.
(39) Nakamura, J.; et al. Formation of a hybrid surface of carbide and graphite layers on Ni(100) but no hybrid surface on Ni(111). *Surf. Sci.* **1989**, *222* (1), L809−L817.
(40) Pukite, P. R.; Lent, C. S.; Cohen, P. I. Diffraction from stepped surfaces: II. Arbitrary terrace distributions. *Surf. Sci.* **1985**, *161* (1), 39−68.
(41) Tinkham, B. P.; et al. Nucleation, coarsening and kinetic scaling of two-dimensional islands on GaSb(001). *Surf. Sci.* **2007**, *601* (3), 814−821.
(42) Michely, T.; et al. Inversion of growth speed anisotropy in two dimensions. *Phys. Rev. Lett.* **1993**, *70* (25), 3943.
(43) Ovesson, S.; Bogicevic, A.; Lundqvist, B. I. Origin of Compact Triangular Islands in Metal-on-Metal Growth. *Phys. Rev. Lett.* **1999**, *83* (13), 2608−2611.